

Specific Features of Formation of Laser-Induced Periodic Surface Structures on Ge₂Sb₂Te₅ Amorphous Thin Films under Illumination by Femtosecond Laser Pulses

Sergey Kozyukhin,* Mikhail Smayev, Vladimir Sigaev, Yuri Vorobyov, Yuliya Zaytseva, Alexey Sherchenkov, and Petr Lazarenko

This article presents the results of irradiation treatment by the 180 fs laser pulses at the wavelength of 1030 nm of Ge₂Sb₂Te₅ amorphous thin films. It is shown that high-quality laser-induced periodic surface structures (LIPSS) are formed at certain parameters of irradiation with a period corresponding to the laser wavelength. A distinctive feature of the observed LIPSS is the alternation of amorphous and crystalline regions corresponding to the ridges and valleys of the periodic structures which are perpendicular to the polarization of the femtosecond light beam. These surface crystalline–amorphous alternating structures are characterized by significantly less pronounced surface relief than for previously observed LIPSS formed by femtosecond laser pulses at the wavelength of 515 nm. Possible mechanisms are considered for the LIPSS formation including the formation of surface plasmon polariton and its subsequent interference with the incident beam resulting in spatial modulation of the temperature on the film surface. As the results indicate, the formation of alternating structure has a threshold nature with the threshold laser fluence for LIPSS formation depending logarithmically on the number of laser pulses, which is attributed to the transient nature of the crystallization process.

switching property, PCMs have been demonstrated to be promising for application in nonvolatile electronic memory devices.^[2,3] The promising PCMs, like Ge–Sb–Te-based alloys (GST), possess unique properties such as high crystallization speed, prominent optical reflectivity and electrical resistivity contrast, excellent reversibility, large number of switching cycles, and high archival lifetimes of more than 10 years.^[4]

One of the key problems of PCMs is the amorphous-to-crystalline phase transition because it is a much slower process relative to other operations in PCM devices, such as reading (READ) or recording (RESET). One of the advanced research directions to improve the crystallization rate is the use of pulsed lasers. So, ultrafast switching behavior relying on nonthermal phase transitions in GST superlattices, triggered by an ultrashort laser pulse, has been proposed in refs. [5,6]. Nevertheless, the understanding of certain material properties and physical mechanisms of PCMs, as well as developments based upon them, broadens the perspective for future applications.


In addition, light–GST material interaction is accompanied by the appearance of a series of effects, such as laser crystallization,^[7] recrystallization,^[8] reamorphization,^[9,10] whole or partial material ablation, and formation of laser-induced periodic surface structures (LIPSS or ripples).^[11–16] In the last case, the possibility to make phase transitions of GST with comparative ease leads to the formation of LIPSS with combined phase states – amorphous and crystalline ones.^[11,13–16] It should be noted that

1. Introduction

Phase-change materials (PCMs) exist in two different stable states, crystalline and amorphous, which exhibit distinctly different physical properties. The most significant feature of this material class is the ability to switch repeatedly and rapidly between these states through heating or cooling. By utilizing the nonvolatility of the optical reflectivity switching property, PCMs have already been applied in commercial rewritable optical storage media such as DVDs and Blu-Ray discs.^[1] Recently, based on the nonvolatility of the large contrast in the electrical resistance

Prof. S. Kozyukhin
Kurnakov Institute of General and Inorganic Chemistry
RAS
Leninsky Pr., 31, Moscow 119991, Russia
E-mail: sergkoz@igic.ras.ru

Dr. M. Smayev, Prof. V. Sigaev
Mendeleev University of Chemical Technology of Russia
Miusskaya Sq., 9, Moscow 125047, Russia

 The ORCID identification number(s) for the author(s) of this article can be found under <https://doi.org/10.1002/pssb.201900617>.

Dr. M. Smayev
Lebedev Physical Institute
RAS
Leninsky Pr., 53, Moscow 119991, Russia

Dr. Y. Vorobyov
Ryazan State Radio Engineering University
Gagarin St., 59/1, Ryazan 390005, Russia

Y. Zaytseva, Prof. A. Sherchenkov, Dr. P. Lazarenko
National Research University of Electronic Technology
Bld. 5, Pas. 4806, Zelenograd 124498, Russia

DOI: 10.1002/pssb.201900617

the ripples attract the attention currently because many researchers see them as an alternative to lithography process, for example.^[17–19] On the one hand, accordingly, the nature of this phenomenon must be well understood to reproducibly obtain LIPSS on a large surface; on the other hand, achieving control over nanostructure formation remains difficult because of high sensitivity of this process to the type of material and laser irradiation parameters that hinder reproducibility and uniformity of periodic patterns.

One of the crucial components for LIPSS formation is the use of a high loss medium; therefore, the bandgap of material is a key parameter.^[20] On the surface of opaque materials, the normal low-spatial frequency LIPSS (coarse ripples) are common for pulsed and continuous laser radiation, and their period, Λ , is independent of pulse duration from femtoseconds to hundreds-of-nanoseconds; on the surface of transparent materials high-spatial frequency LIPSS (fine ripples) are pronounced; however, at certain conditions low-spatial frequency LIPSS can also be observed (see, e.g., review^[21] and references therein).

We have previously observed the formation of high- and low-spatial frequency LIPSS on the surface of amorphous $\text{Ge}_2\text{Sb}_2\text{Te}_5$ (GST225) thin films at a wavelength λ of 515 nm (2.4 eV) that corresponds to absorption coefficient $\alpha = 5.8 \times 10^5 \text{ cm}^{-1}$ and light penetration depth of about 15 nm at a film thickness of about 120 nm.^[14] In the present study, we used the laser with $\lambda = 1030 \text{ nm}$ (1.2 eV), and this wavelength corresponds to $\alpha = 1.2 \times 10^5 \text{ cm}^{-1}$ and light penetration depth of about 83 nm at the same film thickness. In both cases the photon energy at the wavelength of irradiation was larger than the bandgap: $h\nu > E_g$. For GST225 this value is varied in the range from 0.63 to 0.75 eV for amorphous state depending on the conditions of thin films preparation and the calculation algorithm; for crystalline state, the value is less and varies from 0.29 to 0.62 eV.^[22] In this study, we analyze how a change in femtosecond laser wavelength affects the ripple parameters at constant parameters of thin films. The knowledge of specific features of LIPSS formation under various femtosecond light conditions allows one to shed light into the mechanism of fine surface structuring of PCMs.

2. Results

X-ray diffraction (XRD) pattern shows broad halo which corresponds to amorphous phase (Figure 1a), and this result correlates with our transmission electron microscope (TEM) and scanning

electron microscope (SEM) data. The Auger electron spectroscopy (AES) proves the uniform distribution of elements across the GST film (Figure 1b). The Raman spectrum recorded at room temperature presents a contour typical for the amorphous GST225 phase; in this case, a characteristic double-humped structure in the range of $100\text{--}170 \text{ cm}^{-1}$ is observed (Figure 1c).

Based on these results, we concluded that as-deposited films are amorphous with uniform distribution of the elements across the thin film thickness, and the composition corresponds to GST225.

The summarized optical microscope (OM) image of the GST225 amorphous film illuminated by the femtosecond laser beam is shown in Figure 2, where the y -axis represents the variation of average laser fluence (F_{AVG}) (seven steps in the range from 1.4 to 21.3 mJ cm^{-2} with different intervals) and the x -axis shows the variation of the pulse number (N) (13 steps in the range of $1\text{--}10^6$ number of pulses). As can be seen from the image, there are several types of marks. Gray background and gray areas inside bright spots correspond to the amorphous phase. We identify bright marks (e.g., mark K on Figure 2) as full crystalline areas because the higher refractive index of crystalline GST225 in the visible range determines its greater reflectivity and, correspondingly, lighter color in OM.^[23] One can see the intermediate marks also which we identified as a mixture of amorphous and crystalline states (mark L on Figure 2). Black marks (mark G) correspond to material ablation process. All these marks require a careful study; however, here we have focused our attention on the ripples that appear in the area indicated by the dashed line in Figure 2.

Figure 3 shows four different ripple images obtained by various methods. It should be noted that the wave vector of the modulation of the surface relief is always parallel to the electric field of the laser beam. We observed that at the polarization plane rotation, ripples also rotate remaining perpendicular to the light field.

First, it can be seen that the ripple period Λ is about $1 \mu\text{m}$, which is close to the laser wavelength, i.e., $\Lambda = \lambda$ (Figure 3a). Thus, we observe the formation of low-spatial frequency LIPSS which are characterized by the ratio $\Lambda/\lambda = 1$. Second, the height difference between the valley and the ridge is several nanometers only, namely, 2–3 nm, according to the atomic force microscopy (AFM) data (Figure 3b, central panel). Note that this value is more than the roughness of the as-deposited amorphous film, but significantly less than the height of the ripples observed in the similar film after the femtosecond laser irradiation with $\lambda = 515 \text{ nm}$, where the 20 nm height ripples were observed.^[14]

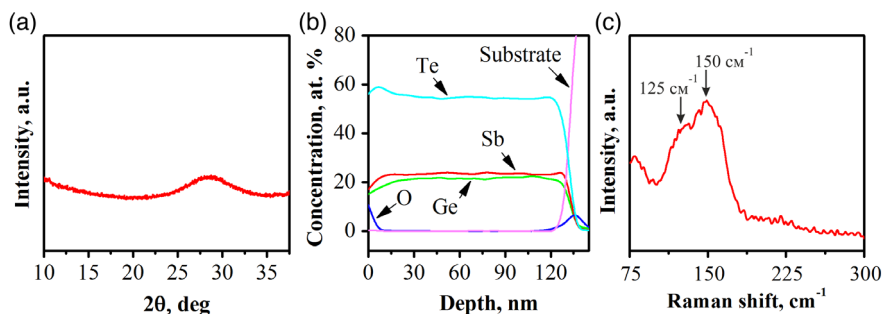


Figure 1. a) XRD pattern, b) distribution of the elements across the thin film thickness, and c) Raman spectrum of as-deposited GST225 films.

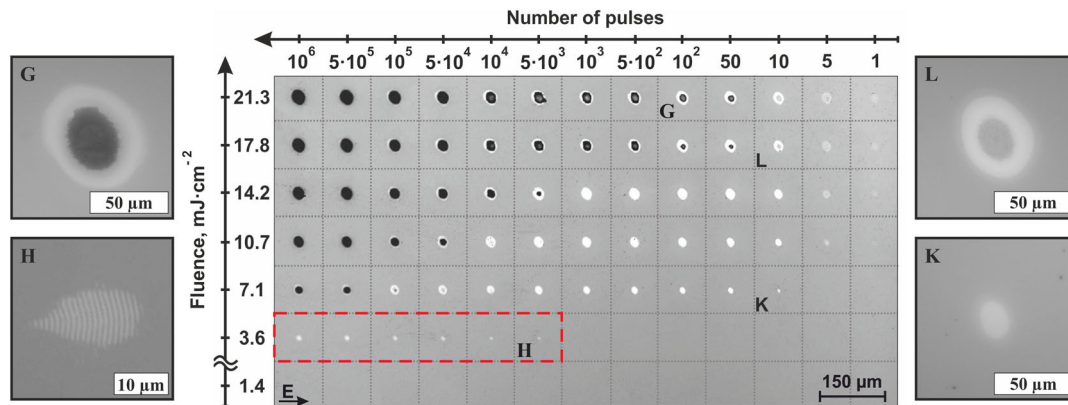


Figure 2. OM image for GST225 amorphous film illuminated by the femtosecond laser pulses with a number of pulses in the range from 1 to 10^6 and average laser fluence ranging from 1.4 to 21.3 mJ cm^{-2} . **E** is the light field vector of the laser beam. The squares labeled by capitalized letters show various processes on the surface of the film. Spot **G** corresponds mainly to the laser ablation; spot **H** shows the appearance of periodic structure; spot **L** demonstrates the crystalline ring with reamorphized central part; spot **K** corresponds to the crystallized region.

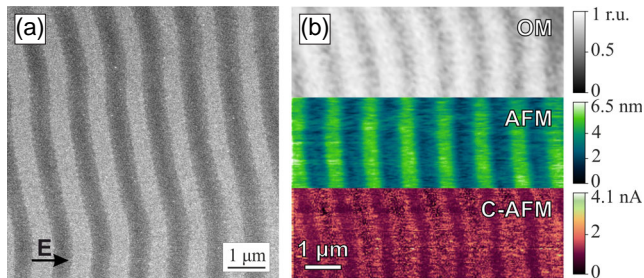


Figure 3. The results of the microscopy studies: a) the SEM image, and b) the overlay of images, obtained using OM, AFM in topography mode, and conductive AFM from the same spot for the mark **H** on Figure 2 ($F_{\text{AVG}} = 3.6 \text{ mJ cm}^{-2}$, $N = 5 \times 10^3$). **E** is the light field vector of the laser beam.

We assume that the formation of such low profile ripples is due to the fact that the light penetration depth is comparable with the film thickness. The spatial concentration of laser radiation in a thinner surface layer (15 nm in ref. [14] and 85 nm in current study due to different laser wavelengths) leads to the formation of ripples with a strongly pronounced relief—the heights of the ripples are 20 and 2 nm, respectively. We suppose that the amplitudes of the initial surface inhomogeneities were approximately the same in both cases because we used the same thin films, and they are not very important for the formation of ripples,^[20] but the laser wavelength affects the absorbed and scattered power of the laser radiation and, accordingly, the feedback coupling. Thus, it can be assumed that the laser wavelength determines not only the ripple period in accordance with the equation $\Lambda = \lambda / (1 \pm \sin \theta)$ (where θ is the incidence angle),^[21] but also their relief.

Third, the experimental data from OM and C-AFM (Figure 3b) suggest that for the observed alternating surface structures the valleys have a lighter color image in the OM and conduct electric current better than the ridges. Also, the striped contrast in SEM image (Figure 3a) can be interpreted in terms of the formation of

regions with different resistance and, therefore, with different secondary electron emission coefficients. It gives reason to suggest that the valleys consist of the crystalline phase, whereas the ridges remain amorphous during laser irradiation.

To understand the crystallite growth process in the GST after the femtosecond pulse laser irradiation, the microstructure evolution was examined by TEM. Figure 4 shows TEM images and fast Fourier transform (FFT) patterns of the film after femtosecond pulse laser irradiation with the average fluence of 3.6 mJ cm^{-2} . In Figure 4c, a cross section of the TEM specimen is shown providing evidence of two different regions inside the irradiated film (the top Pt layer was used to prevent structural damage of the GST film during the TEM specimen preparation). The corresponding FFT patterns in Figure 4d,e are typical for crystalline and amorphous structures of GST. Analysis of the FFT patterns showed that upon irradiation a cubic GST phase with a lattice parameter of 6.0 \AA is formed.

Crystalline grains developed within the amorphous GST matrix after laser irradiation have an oval profile (Figure 4b). The depth of the crystallized region can reach about 55 nm. The radius of curvature is approximately $0.9 \mu\text{m}$ at the edge of the spot and $1.5 \mu\text{m}$ in its central part. The difference in these values is related to the different lengths of the crystalline regions.

The represented results correlate well with the results shown in Figure 3, namely, there are periodic crystalline regions in the amorphous matrix, which is confirmed by FFT patterns. Higher reflectivity of the crystalline phase and its better conductivity explain the periodic features observed using OM and C-AFM. These crystalline regions are located at a few nanometers below the surface of the amorphous film, so that they form valleys. We assume that the relative height changes at the level of several percent is due to the increase of about 7% in the density of the crystalline phase in comparison with the amorphous one,^[24] which leads to the compression of these material regions. A characteristic and quite interesting feature of this phenomenon is that there are no mechanical defects or damages such as cracks, for example, on the border between these two areas in the film.

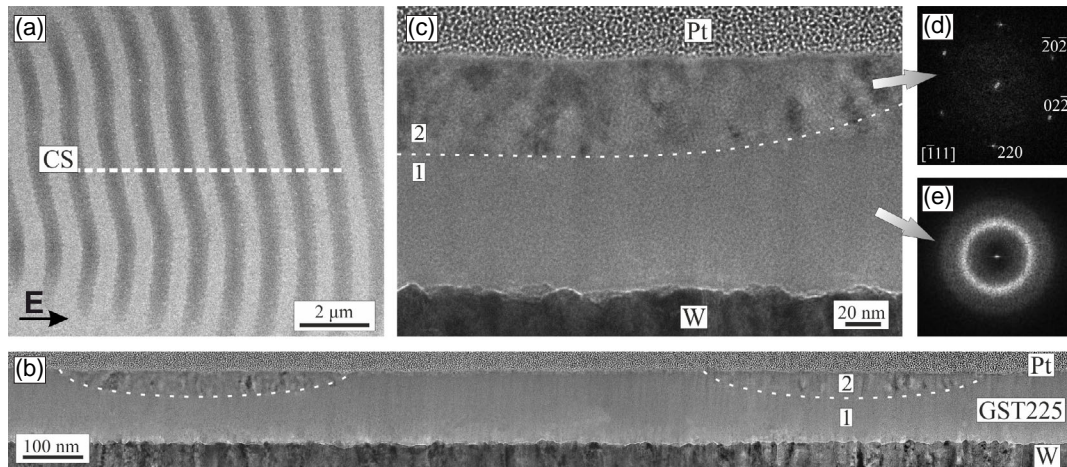


Figure 4. The results of the electron microscopy analysis: a) the SEM image for the mark H on Figure 3 (CS, cross section place); b,c) TEM images of the ripples profile at different scales; d,e) Fourier transform patterns for the indicated areas. The image (d) corresponds to crystalline GST structure; the image (e) corresponds to amorphous GST structure. E is the light field vector of the laser beam.

This indicates that the amorphous structure of GST225 is sufficiently flexible and labile.

Figure 5 shows the evolution of the irradiated area with an increase in the number of pulses at the constant fluence. It can be seen that ripples begin to form starting with 5×10^3 pulses, and the area covered by ripples is increased with rise in the number of pulses. A characteristic feature of this process is the appearance of a uniform dark gray area in the center of the mark at a higher number of laser pulse repetitions. Considering previous results we can conclude that a continuous crystalline area forms in the center of an illuminated area in the case of large values of the number of pulses.

3. Discussion

The growth of the ripples area with the increase in the number of pulses together with the Gaussian distribution of local light intensity across the laser spot implies that the local fluence necessary for the formation of the ripples decreases. To extract the threshold value of this local laser fluence, the following procedure was applied. The area covered by ripples was determined from an optical (or SEM) image and then the value of local laser fluence F_{th} was found such that the values higher than F_{th} cover the same area on the image of the laser beam. Obtained results are shown in **Figure 6**.

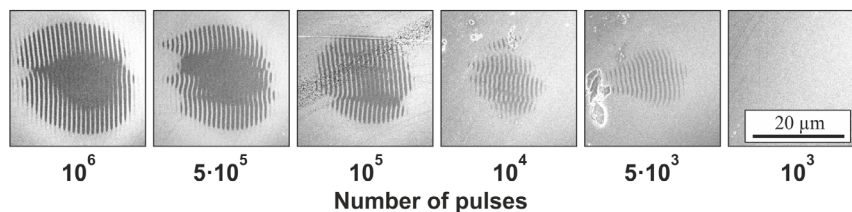


Figure 5. SEM images for the GST225 amorphous film illuminated by femtosecond laser pulses with a number of pulses from 10^3 to 10^6 at the constant average fluence of 3.6 mJ cm^{-2} .

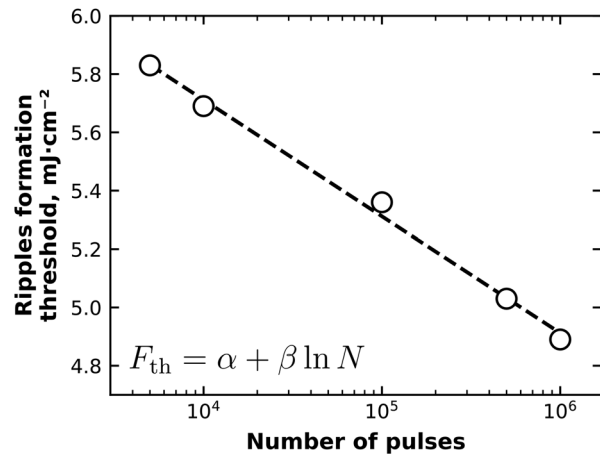


Figure 6. The dependence of the local laser fluence F_{th} needed for ripples formation on the number of laser pulses N (α and β are parameters of the linear approximation given as the dashed line).

The dependence of the threshold fluence on the logarithm of the number of pulses exhibits sufficiently linear behavior demonstrated by the dashed line in **Figure 6**. In other words, the number of pulse repetitions, which is necessary to produce the ripples, is a negative exponential function of the local laser

fluence. This, in turn, suggests that some positive feedback may be involved in lowering the threshold for ripples formation with the increase in the number of pulses.

Crystallization process, which governs the formation of ripples in the initially amorphous film (Figure 4), comprises nucleation of individual crystallization sites and their subsequent growth. Nucleation process is transient in nature,^[25] and it means that the development of stable nuclei in response to sudden changes (e.g., provided by an external influence, like a laser pulse) takes some time (or, in our case, some considerable number of laser pulses). Decrease in this time period (often called *incubation time* in the literature) at higher temperatures is a common property of the nucleation behavior of noncrystalline solids^[25] as well as GST itself.^[26] Higher values of laser fluence provide greater heating effect; accordingly, a fewer number of laser pulses becomes sufficient to establish the stable nuclei. Due to Gaussian distribution of light intensity in the laser beam, points that are more distant from the beam axis are subjected to a lower value of laser fluence. Therefore, more pulses are needed to provide appropriate conditions for their crystallization, and that is why we observe gradual growth of modified areas in Figure 5.

Periodic surface structures can appear during the interaction of light pulses with the surfaces of materials with different dielectric characteristics (metals, transparent and absorbing semiconductors, or dielectrics).^[21] Moreover, periodic structures were observed under the influence of both long light pulses (with a duration of more than 10^{-11} s, significantly exceeding the characteristic times of electron–phonon relaxation) and when exposed to ultrashort light pulses. The appearance of periodic structures can be explained by the formation of a surface electromagnetic wave as a result of the interaction of light pulses with a matter and subsequent interference of this surface wave with the initial beam.^[20,27]

A specific feature of an ultrashort pulse interaction with a matter is its ability to change the dielectric properties of the material due to the response of the electronic subsystem, whereas other processes (in particular, associated with the transfer of energy to the lattice) start after the end of the light pulse. Although initially amorphous GST225 is a semiconductor,^[28] when exposed to ultrashort pulses, an increase in the density of free carriers is possible, which at a certain threshold value will lead to “metallization”^[29–33] of the GST surface. In this case, the real part of the dielectric permittivity ϵ changes its sign to negative and favorable conditions appear for the formation of surface waves.

The ripples described in the current work with a period equal to the wavelength and oriented perpendicular to the polarization of the light field are explained by the appearance of the surface plasmon polariton (SPP),^[29–32] that is surface wave orthogonal to the interface (transverse-magnetic mode of electromagnetic radiation). As a result of the interference of the incident beam and the electromagnetic wave of SPP, a spatial modulation of the temperature of the surface layer occurs, leading to spatially modulated GST crystallization. This periodic phase pattern would remain still between laser pulses, further facilitating the coupling of incident light into the SPP after each pulse and, therefore, interference pattern formation as well. Furthermore, the absorption coefficient of the crystalline GST is higher than that of the amorphous one; emerging of crystalline phase during LIPSS formation therefore increases the local heating effect of laser pulse

and promotes the crystallization process. Therefore, the positive feedback during multipulse excitation may indeed take place in the investigated phenomena.

This qualitatively differs from the surface structures that arise upon irradiation of GST films with femtosecond pulses with a wavelength of 515 nm^[14] which, depending on the light field parameters, were formed both perpendicular to the light polarization and parallel to it. Ripples parallel to the light field can be explained by the formation of the waveguide mode of the surface wave (a transverse-electric mode of electromagnetic radiation polarized parallel to the interface) and due to the formation of a layered structure in which a layer with negative ϵ is separated from the surface by a layer with positive permittivity.^[29,30] An order of magnitude higher value of relief modulation of LIPSS formed under 515 nm laser excitation^[14] allows to assume that, in contrast to the current study, the ablation process was involved, which is also characterized by a pronounced dependence on the number of laser pulses. However, published data indicate the dependence of the threshold fluence for ablation on the pulse number in the form of a power law^[34,35] or decaying exponent.^[36,37] Our results show rather logarithmic behavior of F_{th} on N (see Figure 6). This again demonstrates the underlying differences between processes of LIPSS formation on the surface of GST under excitation of lasers of different wavelengths.

4. Conclusions

We observed the formation of two-phase low-spatial frequency LIPSS on the surface of the initial amorphous thin films of GST225 composition under illumination by femtosecond laser pulses with the wavelength of 1030 nm. We showed that the ripple formation is a common phenomenon in PCM materials of GST225 composition.

We have determined the ripple parameters by several independent methods (optical microscopy, SEM, TEM, AFM, etc.) which correlate with each other. The ripples were oriented perpendicular to the light field of femtosecond beam; their period was close to laser wavelength (about 1 μ m). It was found that the valleys consist of the crystalline phase, whereas the ridges remain amorphous after femtosecond laser illumination. The height difference between the valley and the ridge is about 2 nm, whereas in previous work the 20 nm height ripples were observed at irradiation of the similar film with $\lambda = 515$ nm. As our results indicate, the formation of ripples has a trigger nature and begins with a certain threshold fluence in the case of a constant number of laser pulses. It is shown that an increase in the pulse number leads to an exponential decrease in the threshold fluence, which is explained by the presence of positive feedback in the studied system. The difference between ripples heights can be explained by the different light penetration depths. Identified features of ripple formation are important for better understanding the nature of the phenomenon and possible future applications.

5. Experimental Section

Thin films of the $\text{Ge}_2\text{Sb}_2\text{Te}_5$ composition were prepared by DC magnetron sputtering at room temperature. The pressure of Ar^+ ions during the process was 5×10^{-3} Torr; the sputtering power was 100 W. Films growth

rate was 24 nm min^{-1} . The films were deposited on W (200 nm)/TiN (50 nm)/SiO₂ (1 μm)/Si (substrate) multilayer structures. The requirements for melting point, thermal stability, and electrical conductivity explained the choice of tungsten as a contact layer for the GST225 thin film. The main role of the TiN layer was to serve as an adhesion sublayer for the tungsten. Silicon was used as a substrate, covered by wet thermal silicon oxide.

The thicknesses of GST films were controlled by the AFM (NT-MDT Solver Pro) and were 120 nm. The surface roughness of the as-deposited thin film was determined as root mean square (RMS) of the height according to ISO 25178 and was $0.34 \pm 0.01 \text{ nm}$.

The phase state of thin films was determined by XRD analysis using a diffractometer (Rigaku Smart Lab) with Cu K α_1 ($\lambda = 1.5406 \text{ \AA}$) radiation. The diffraction angle (2θ) was scanned from 10° to 40° with a step size of 0.001° and a scanning speed of 1° min^{-1} .

The distribution of the elements across the sample thickness was investigated by Auger (AES, PHI-660, PerkinElmer Inc.) and time-of-flight secondary ion mass (TOF-SIMS, TOF.SIMS 5, IonTOF) spectroscopies. Depth profiles of elements atomic concentrations were obtained by AES method using sample sputtering by Ar⁺ ion beam (2 kV, 0.35 μA). Between the etching steps, the surfaces of samples were analyzed by the electron beam (5 kV, 20 nA). The diameter of the analyzed area was 100 μm . Concentrations of elements were determined in accordance with the model of homogeneous distribution of components using element sensitivity coefficients method. The TOF-SIMS investigation was performed using Bi⁺ analysis beam (30 kV, 15 pA) and Cs⁺ sputtering beam. Accelerating voltage for etching was chosen to be 500 V for optimal depth resolution, due to the fact that in this etching regime an additional relief on the sample does not appear. The sputtering raster area was $300 \times 300 \mu\text{m}^2$ and the analysis field was $100 \times 100 \mu\text{m}^2$.

We used an Yb:KGW femtosecond laser system (Pharos SP, Light Conversion) emitting pulses at the wavelength of 1030 nm with a duration of 180 fs and repetition rate of 200 kHz. The normally incident laser beam was focused with a lens with a focal distance of 75 mm. The light field polarization was linear and could be rotated around the optical axis using a halfwave plate controlled from the PC.

The films were placed onto an Aerotech ABL1000 air-bearing high precision 3D translation stage and shifted from the beam focus into the diverging beam at a distance of 1.2 mm. The beam profile was recorded using CCD camera Spiricon SP620U (Ophir). The beam diameter at the sample plane was about 65 μm (1 e^{-2}). During the light exposure, the films were moved in the plane perpendicular to the light beam. At the specific positions, the stage stopped and the laser system delivered to the sample fixed number of femtosecond pulses at a certain value of average energy density fluence (the ratio of pulse energy to beam spot area).

AFM was used to investigate the topography of the thin films. Conductive AFM (c-AFM, Ntegra, NT-MDT Spectrum Instruments) at 0.5 V bias voltage was used to map electrical conductance across the modified areas of the experimental samples.

For Raman study, we used LabRAM HR Evolution spectrometer (HORIBA) with 514 nm excitation wavelength, 600 mm^{-1} diffraction grating, $100\times/0.9\text{NA}$ objective, and a beam spot size of 1 μm in diameter. Cooled CCD matrix detector was used for spectra recording. The excitation power was limited to 0.1 mW to avoid heating effect during the acquisition of spectra.

Thin films were studied using a TEM/SEM Titan 80-200 (FEI) and NVision 40 (Carl Zeiss). For the TEM analyses, we used in situ lift-out method of cross-sectional specimen preparation (FEI Helios NanoLab 650 dual-beam workstation). Energy-dispersive X-ray spectroscopy (EDX) of the TEM was used for the local chemical microanalysis.

Acknowledgements

The study was supported by the Russian Foundation for Basic Research (20-03-00379) and the Ministry of Science and Higher Education of the Russian Federation. The Raman, Auger, SEM, and TEM experiments were supported by the Russian Foundation for Basic Research (project number 18-33-20237\18). The studies were performed using equipment of

Regional Centre for Probe Microscopy of RSREU, Core facilities centers "Diagnostics and modification of microstructures and nanoobjects," "MEMS and electronic components," and "STI Sensory" of MIET.

Conflict of Interest

The authors declare no conflict of interest.

Keywords

femtosecond laser irradiation, Ge₂Sb₂Te₅, GST225 thin films, laser-induced periodic surface structures, phase change memory

Received: September 29, 2019

Revised: May 21, 2020

Published online:

- [1] M. Wuttig, N. Yamada, *Nat. Mater.* **2007**, *6*, 824.
- [2] H. S. P. Wong, S. Raoux, S. Kim, J. Liang, J. P. Reifenberg, B. Rajendran, M. Asheghi, K. E. Goodson, *Proc. IEEE* **2010**, *98*, 2201.
- [3] M. H. R. Lankhorst, B. W. S. M. M. Ketelaars, R. A. M. Wolters, *Nat. Mater.* **2005**, *4*, 347.
- [4] S. Raoux, W. Wetnic, D. Ielmini, *Chem Rev.* **2010**, *110*, 240.
- [5] M. Hada, W. Oba, M. Kuwahara, I. Katayama, T. Saiki, J. Takeda, K. G. Nakamura, *Sci. Rep.* **2015**, *5*, 13530.
- [6] R. E. Simpson, P. Fons, A. V. Kolobov, T. Fukaya, M. Krbal, T. Yagi, J. Tominaga, *Nat. Nanotechnol.* **2011**, *6*, 501.
- [7] X. Sun, M. Ehrhardt, A. Lotnyk, P. Lorenz, E. Thelander, J. W. Gerlach, T. Smausz, U. Decker, B. Rauschenbach, *Sci. Rep.* **2016**, *6*, 28246.
- [8] P. Rodenbach, A. Giussani, K. Perumal, M. Hanke, M. Dubschlaff, H. Riechert, R. Calarco, M. Burghammer, A. V. Kolobov, P. Fons, *Appl. Phys. Lett.* **2012**, *101*, 061903.
- [9] J. Siegel, W. Gawelda, D. Puerto, C. Dorronsoro, J. Solis, C. N. Afonso, J. C. G. de Sande, R. Bez, A. Pirovano, C. Wiemer, *J. Appl. Phys.* **2008**, *103*, 023516.
- [10] J. Takeda, W. Oba, Y. Minami, T. Saiki, I. Katayama, *Appl. Phys. Lett.* **2014**, *104*, 261903.
- [11] Y. Katsumata, T. Morita, Y. Morimoto, T. Shintani, T. Saiki, *Appl. Phys. Lett.* **2014**, *105*, 031907.
- [12] Y. Li, V. A. Stoica, L. Endicott, G. Wang, H. Sun, K. P. Pipe, C. Uher, R. Clarke, *Appl. Phys. Lett.* **2011**, *99*, 121903.
- [13] S. A. Yakovlev, A. V. Ankudinov, Y. V. Vorobyov, M. M. Voronov, S. A. Kozyukhin, B. T. Melekh, A. B. Pevtsov, *Semiconductors* **2018**, *52*, 809.
- [14] S. Kozyukhin, P. Lazarenko, Y. Vorobyov, A. Baranchikov, V. Glukhenkaya, M. Smayev, A. Sherchenkov, Y. Sybina, A. Polohin, V. Sigaev, *Opt. Laser Technol.* **2019**, *113*, 87.
- [15] M. Garcia-Lechuga, D. Puerto, Y. Fuentes-Edfuf, J. Solis, J. Siegel, *ACS Photonics* **2016**, *3*, 1961.
- [16] Y. Fuentes-Edfuf, M. Garcia-Lechuga, D. Puerto, C. Florian, A. Garcia-Leis, S. Sanchez-Cortes, J. Solis, J. Siegel, *Sci. Rep.* **2017**, *7*, 4594.
- [17] J. Bonse, J. Krüger, S. Höhm, A. Rosenfeld, *J. Laser Appl.* **2012**, *24*, 042006.
- [18] R. Le Harzic, D. Dörr, D. Sauer, M. Neumeier, M. Eppe, H. Zimmermann, F. Stracke, *Opt. Lett.* **2011**, *36*, 229.
- [19] J. Huang, L. Jiang, X. Li, A. Wang, Z. Wang, Q. Wang, J. Hu, L. Qu, T. Cui, Y. Lu, *Nanophotonics* **2019**, *8*, 869.
- [20] S. A. Akhmanov, V. I. Emel'yanov, N. I. Koroteev, V. N. Seminogov, *Sov. Phys. Usp.* **1985**, *28*, 1084.
- [21] R. Buividas, M. Mikutis, S. Juodkazis, *Prog. Quantum Electron.* **2014**, *38*, 119.

- [22] P. Lazarenko, Y. Vorobyov, M. Fedyanina, A. Sherchenkov, S. Kozyukhin, A. Yakubov, A. Kukin, Y. Sybina, I. Sagunova, *Inorg. Mater. Appl. Res.* **2020**, *11*, 330.
- [23] J. Park, S. H. Eom, H. Lee, L. F. Da Silva, Y. Kang, T. Lee, Y. H. Khang, *Phys. Rev. B* **2009**, *80*, 115209.
- [24] K. Wang, C. Steimer, D. Wamwangi, S. Ziegler, M. Wuttig, *Appl. Phys. A: Mater. Sci. Process.* **2005**, *80*, 1611.
- [25] K. F. Kelton, *Solid State Phys.* **1991**, *45*, 75.
- [26] V. Weidenhof, I. Friedrich, S. Ziegler, M. Wuttig, *J. Appl. Phys.* **2001**, *89*, 3168.
- [27] J. E. Sipe, J. F. Young, J. S. Preston, H. M. van Driel, *Phys. Rev. B* **1983**, *27*, 1141.
- [28] *Phase Change Memory: Device Physics Reliability and Applications* (Ed.: A. Redaelli), Springer, Cham, Switzerland **2018**.
- [29] G. A. Martsinovsky, G. D. Shandybina, D. S. Smirnov, S. V. Zobotnov, L. A. Golovan', V. Yu. Timoshenko, P. K. Kashkarov, *Opt. Spectrosc.* **2008**, *105*, 67.
- [30] G. A. Martsinovsky, G. D. Shandybina, Yu. S. Dement'eva, R. V. Dyukin, S. V. Zobotnov, L. A. Golovan', P. K. Kashkarov, *Semiconductors* **2009**, *43*, 1298.
- [31] V. S. Makin, Yu. I. Pestov, R. S. Makin, A. Ya. Vorob'ev, *J. Opt. Technol.* **2009**, *76*, 555.
- [32] J. Y. Derrien, J. Krüger, T. E. Itina, S. Höhm, A. Rosenfeld, J. Bonse, *Appl. Phys. A: Mater. Sci. Process.* **2014**, *117*, 77.
- [33] P. A. Danilov, A. A. Ionin, S. I. Kudryashov, S. V. Makarov, A. A. Rudenko, P. N. Saltuganov, L. V. Seleznev, V. I. Yurovskikh, D. A. Zayarny, T. Apostolova, *J. Exp. Theor. Phys.* **2015**, *120*, 946.
- [34] Y. Jee, M. F. Becker, R. M. Walser, *J. Opt. Soc. Am. B* **1988**, *5*, 648.
- [35] J. Bonse, S. Baudach, J. Krüger, W. Kautek, M. Lenzner, *Appl. Phys. A* **2002**, *74*, 19.
- [36] D. Ashkenasi, M. Lorenz, R. Stoian, A. Rosenfeld, *Appl. Surf. Sci.* **1999**, *150*, 101.
- [37] A. Rosenfeld, M. Lorenz, R. Stoian, D. Ashkenasi, *Appl. Phys. A* **1999**, *69*, S373.